# Mechanisms of phase transformation and creating mechanical strength in a sustainable calcium carbonate cement

**Jesús Rodríguez-Sánchez[1,*], Teresa Liberto[2], Catherine Barentin[2,3] and Dag Kristian Dysthe[1].**

[1.] Physics of Geological Processes (PGP), The NJORD Centre, Department of Physics, University of Oslo, PO Box 1048 Blindern, Oslo, Norway.

[2.] Institut Lumière Matière, F-69622, Université Claude Bernard Lyon 1, CNRS, Villeurbanne, France.

[3.] Institut Universitaire de France, France.

* **E-mail:** j.r.sanchez@fys.uio.no

**Abstract**

*Calcium carbonate cements have been synthesized by mixing amorphous calcium carbonate and vaterite powders with water to unravel the mechanisms of creating mechanical strength during the setting reaction. In-situ XRD was used to monitor the transformation of ACC and vaterite phases into calcite. Unlike this transformation of crystals suspended in a stirred solution, the transformation in the cement is controlled by vaterite dissolution. The supersaturation within the cement paste, Ω, depends not only on the bulk free energy difference of the phases, ΔG, but also on the grain size evolution. Among the strengthening mechanisms, an initial geometric reorganization of $CaCO_3$ particles has been identified by rheological measurements; followed by the formation of an interconnected network of calcite crystals that increases in strength as the crystals grow and form bridges among them. All compositions yield microporous calcite structures with diverse transformation history, crystal bridging efficiency, and hence final mechanical properties.*

**Keywords**: Calcium carbonate cement, Setting reaction, (Re)crystallization kinetics, Cement strengthening, Crystal bridging.

## 1. Introduction

Due to the carbon footprint of ordinary Portland cement (OPC) there has been an increased interest in alternative hydraulic binders [1–4]. Inspired by the outstanding mechanical properties of limestone, which is mainly composed of calcium carbonate ($CaCO_3$), alternative production paths to form calcium carbonate binders have been investigated [1,5,6], the most famous being the Calera carbonation process [7]. Another path to prepare pure $CaCO_3$ cements is of special interest as a model system: Combes and co-workers [5,6] mixed water with two metastable $CaCO_3$ phases. One of them is the highly reactive amorphous calcium carbonate, ACC, while the other is one of the metastable crystalline phases, either vaterite, V, or aragonite, Ar. The polymorphs ACC and V or A recrystallize into the most stable polymorph, calcite, during the setting of the cement. Recrystallization of $CaCO_3$ polymorphs has received much attention the later years [8–16] due to the importance of $CaCO_3$ in industry [17], climate [18], Biomineralization [19] and geology [20]. This large body of knowledge on recrystallization mechanisms has yet to be put into the context of $CaCO_3$ cement setting. In this paper, we compare

Preprints (www.preprints.org) | NOT PEER-REVIEWED | Posted: 23 October 2018 doi:10.20944/preprints201810.0526.v1

$CaCO_3$ setting reactions with the transformation mechanisms in other settings and then we compare this to the development in rheology of the $CaCO_3$ cement paste during setting.

$CaCO_3$ polymorphic transformation follows an energetically downhill sequence: ACC → Vaterite → Aragonite → Calcite [21]. However, indirect transformations or more complex mechanisms out of the classical nucleation theory (CNT) may also occur [22], resulting on unknown activation energies and growth/dissolution rates. Multiple studies have been carried out to unravel the mechanisms and the energetics among the $CaCO_3$ polymorphic transformations in solutions, both computational and experimental [9–11,21]. For example, *Rodriguez-Blanco et al*. [11] and *Bots et al.* [12] found that hydrated ACC transforms into an intermediate anhydrous ACC before forming vaterite; then, vaterite transforms to calcite (at temperatures below 40 °C) via a dissolution and reprecipitation mechanism with the reaction rate controlled by the surface area of calcite. However, a cement paste represents a more complex challenge since the amount of available water plays a key role as an external mediator/inducer of the transformation [11]. The liquid phase remains saturated with respect to a different polymorph depending on both their solubility and their relative existence within the paste [23], causing the driving force of the transformation to vary with time. Moreover, the paste may experience evaporation at the paste/air interface depending on the environmental conditions during setting. Hence, a better understanding of these simultaneous transformations that $CaCO_3$ pastes undergo during the setting reaction are still necessary.

Considering that the properties of hardened $CaCO_3$ cements are a result of the (re)crystallization that the paste undergoes when the solid reagents are mixed with water, it is of crucial importance to correlate these phase transformations with the evolution of the viscoelastic properties of the paste during maturation to unravel the strengthening mechanisms and their kinetics [24,25].

In the present study, sustainable 100% pure calcium carbonate cements have been synthesized following "Combes' method" [6] to investigate: i) the transformation kinetics of each phase (ACC, vaterite and calcite) within a paste system and ii) their structural built up mechanisms during setting. To address these effects, *in-situ* X-ray diffraction (XRD) scans and rheological measurements have been carried out, respectively, over cement pastes with dissimilar mixture design. The combination of these results aims to build up a better understanding of the relationship between $CaCO_3$ phase transformations and strengthening kinetics, not only for pure $CaCO_3$ cements but for other carbonated materials with important implications in many fields.

## 2. Materials and methods

$CaCO_3$ cement samples with diverse mixture design have been prepared. Both the composition and the (re)crystallization kinetics of each $CaCO_3$ phase (ACC, vaterite and calcite) along setting and hardening processes have been studied by *in-situ* time-lapse X-ray diffraction (XRD). Then, the effect of ACC and vaterite (re)crystallization on the viscoelastic properties of the pastes have been quantified by rheological measurements.

*Preprints* (www.preprints.org) | NOT PEER-REVIEWED | Posted: 23 October 2018 doi:10.20944/preprints201810.0526.v1

*2.1. Synthesis of $CaCO_3$ polymorphs*

The preparation of $CaCO_3$ cements requires the synthesis of different calcium carbonate polymorphs in order to design the initial cement mixture [6]. Accordingly, both ACC and vaterite phases were precipitated by mixing calcium chloride ($CaCl_2 \cdot 6H_2O$, Sigma Aldrich) and sodium carbonate ($Na_2CO_3$, Sigma Aldrich) equimolar (0.5 M) solutions, prepared with ultrapure Milli-Q water (18.2 MΩ cm), at room temperature using a magnetic stirrer set at 400 rpm. Following *Ogino et al.* [8] we used reaction time 10 sec for ACC and 30 min for vaterite. To wash off any dissolved sodium chloride (NaCl), the $CaCO_3$ precipitates were rinsed with deionized water and ethanol, using a filtering kit and 0.5 μm pore-size filter papers (Millipore, USA). Subsequently, the $CaCO_3$ precipitates were flushed with liquid $N_2$ to stop the recrystallization of these metastable phases. The frozen precipitates were lyophilized (Alpha 1-4 LD plus, Martin Christ, Germany) for 48 h at 0.05 mbars and -50 °C and stored in a freezer (-22˚C) with additional silica powder bags to keep them as dry as possible [13] prior to cement manufacturing.

The precipitates were scanned by X-ray diffraction (XRD) (Bruker D8 Discover X-ray diffractometer) to identify the crystalline phases present using Cu Kα radiation (30 mA and 40 kV) and recording $2\theta$ angles from 20 to 50° at a 0.04 $s^{-1}$ sweep rate. Additionally, they were imaged with scanning electron microscopy (SEM) (Hitachi SU5000 Field-Emission; 1kV acceleration voltage and 3.0 mm working distance).

*2.2. In-situ XRD analysis during setting and hardening*

To quantify the composition and the (re)crystallization kinetics of $CaCO_3$ cement pastes along setting and hardening processes we have used *in-situ* time-lapse X-ray diffraction (XRD) (Bruker D8 A25 X-ray diffractometer). Five $CaCO_3$ cement pastes were made up of mixtures of ACC and vaterite powders in different weight ratios (wt.%): 1:0, 1:1, 1:2, 1:3 and 0:1 wt.%, with a solid volume concentration, $\Phi$, equal to 46%. This concentration was deduced from the total powder weight and ACC, vaterite and water densities. Just after mixing the powders with the liquid phase, the resulting pastes were viscous so easily mouldable for several minutes and they were moulded into the sample holder (disk of 25 mm diameter, 2 mm depth), firmly tamped and covered with a plastic film immediately after mixing with water to avoid drying.

XRD patterns were recorded every 5 min for a maximum of 60 hours using Mo Kα radiation (48 mA and 48 kV) and recording $2\theta$ angles from 10 to 17° at a sweep rate of 0.035 $s^{-1}$. Since the mass of a crystalline phase, $m_i$, is proportional to the area, $A_i$, under its diffraction peak ($m_i \; \alpha \; A_i$), the net area under the main vaterite and calcite diffraction peaks (located at 12.35° and 13.39°, respectively within the range scanned) were calculated using the software Diffrac.Suite EVA (Bruker AXS, USA) for each scan. The mole fractions of each phase, $X_i$, can be calculated from $A_i$ based on two assumptions: The vaterite mole fraction in the first scan is the same as in the initial mixture and in the final scan the cement is pure calcite. Then, the evolution of the mole fractions for vaterite, $X_V(t)$, and calcite, $X_C(t)$, could be determined using the following relations:

Preprints (www.preprints.org) | NOT PEER-REVIEWED | Posted: 23 October 2018 doi:10.20944/preprints201810.0526.v1

$$X_C(t) = \frac{A_C(t)}{A_C(t_f)} \quad \text{and} \quad X_V(t) = X_V(t_0) \cdot \frac{A_V(t)}{A(t_0)} \tag{1}$$

where $t$ represents the time and $X_V\ (t_0)$ the starting vaterite mole fraction which is determined by the mixture design, i.e., either 0, 0.5, 0.66, 0.75 or 1, for the ACC:V 1:0, 1:1, 1:2, 1:3 and 0:1 wt.% pastes, respectively. Moreover, the mole fraction evolution of ACC, $X_{ACC}\ (t)$, could be easily determined since the total mole fractions follow $X_C\ (t)+X_V\ (t)+X_{ACC}\ (t)=1$.

*2.3. Rheological characterization*

*2.3.1. Sample preparation*

$CaCO_3$-cement colloidal suspensions were prepared by dispersion of ACC and vaterite powdered mixtures in distilled water. Three different mixtures were made up by mixing ACC and vaterite powders in different weight ratios (wt.%): 1:1, 1:2 and 1:3, respectively. The selected solid volume concentration, $\Phi$, was 36% based on preliminary tests to determine the suitable concentration range for rheological measurements (Storage modulus, G' > loss modulus, G''). We could not study higher concentrations, $\Phi$, due to some limitations of the rheometer and in particular due to its maximal torque. This concentration was deduced from the total powder weight and ACC and vaterite densities within the paste. The admixture of the solid and the liquid phase was carried out in a vortex stirrer (Ultra Turrax TD300) at 5800 rpm for 20 seconds. This time was checked to be long enough to assure a homogeneous and easily moldable paste without modifying its viscoelastic properties. After the mixing step, the samples were immediately transferred into the rheometer plate and tested.

*2.3.2. Measurement protocols*

The viscoelastic properties of the cement pastes (ACC:V mixtures) were studied using a stress-controlled rotational rheometer (Anton Paar MCR 301) by applying oscillatory deformation. The measurements were carried out using plate-plate geometry (36 and 64 mm, upper and lower diameters, respectively) at room temperature. The gap between the two plates was fixed to 2 mm, aiming to obtain bulk paste properties since it is much larger than the $CaCO_3$ particle diameter. Both plates were covered with sand paper PV 320 (roughness 46 μm) to prevent from slippage [26] and slip at the plate walls was indeed discarded from preliminary shear dynamics studies across the rheometer gap using diffusing-wave spectroscopy (DWS) [27]. In addition, a moisture chamber was used to assure a water-saturated atmosphere and thus dispel any paste drying effect during the data acquisition.

From the measurements, the storage modulus, $G'$, and the loss modulus, $G''$, were extracted as the characterizing parameters of the viscoelastic behaviour. Those are defined by [28]:

$$G^* = G' + iG'' \tag{2}$$

where G* is the complex modulus which corresponds to the ratio between the complex stress, $\sigma^*$, and the complex strain, $\gamma^*$:

$$\sigma^*(t) = G^* \cdot \gamma^*(t) \tag{3}$$

Preprints (www.preprints.org) | NOT PEER-REVIEWED | Posted: 23 October 2018 doi:10.20944/preprints201810.0526.v1

Two different experimental protocols were used. The first one aims at studying the evolution of the ACC and vaterite transformation reaction by measuring the time evolution of the storage modulus ($G'(t)$) during 10 hours. The second one aims at characterizing the elastic properties of the $CaCO_3$ cement pastes after 5 hours of reaction.

*2.3.2.1. Viscoelastic measurements during setting reaction: aging experiment*

To quantify the influence of ACC and vaterite recrystallization into calcite on the macroscopic mechanical properties of pastes, a constant oscillatory deformation, $\gamma$ = 0.003%, was applied to the pastes at the imposed frequency of f = 10 Hz, for several hours, which allows to measure the time evolution of the visco-elastic moduli ($G'$, $G''$) during the setting reaction. These values of strain and frequency ($\gamma$ = 0.003%, f=10 Hz) were chosen small enough to ensure measurements within the linear elastic regime for all the tested pastes, and thus no perturbation of the setting and hardening dynamics of the samples. The measurements started immediately after mixing the solid and the liquid phase, transferring the pastes into the plate-plate geometry and sealing the setup with the moisture chamber.

*2.3.2.2. Characterization of the viscoelastic properties after 5 hours of reaction*

To characterize the viscoelastic properties of the three $CaCO_3$ cement pastes after 5 hours of reaction, amplitude sweep measurements were performed in the oscillatory regime at constant frequency, f = 10 Hz, with increasing stress, $\sigma$ = 1-$10^4$ Pa. In such experiment, the stress is imposed and the resulting strain is measured. At low stresses and low strains, the storage modulus, $G'$, is constant as shown on Figure 7, so the linear storage modulus, $G'_{lin}$, can be estimated precisely. At larger strains, the pastes eventually yield and become liquid-like, making the storage modulus, $G'$, to breakdown. The end of the linear regime, i.e., the onset of plasticity, was characterized by the critical strain, $\gamma_{CR}$, which corresponds to the value of $\gamma$ for which the storage modulus was 10-15% lower than the value in the elastic regime, $G'_{lin}$ [26].

The pastes were prepared as described on Section 2.3.1., transferred into the plate-plate setup, sealed with the moisture chamber and let them to react for 5 hours at static conditions before the measurement started.

## 3. Results and discussion

The synthesized amorphous calcium carbonate, ACC, and vaterite, V, polymorphs, necessary to manufacture $CaCO_3$ cements are introduced. Subsequently, the transformation kinetics of each $CaCO_3$ polymorph within a cement paste system is described and analyzed. Lastly, a correlation between the (re)crystallization kinetics and viscoelastic properties of the pastes is presented and discussed.

*3.1. Characterization of $CaCO_3$ precipitates*

To check the validity of the synthesis protocols described for both ACC and vaterite, the dried precipitates used as starting materials for the different cement compositions are investigated by SEM and XRD. The SEM analysis indicates that ACC precipitates (Figure 1A) consist of equidimensional spherical nanoparticles (<50 nm in diameter) accompanied by rhombohedral crystals of about 50-100

Preprints (www.preprints.org) | NOT PEER-REVIEWED | Posted: 23 October 2018 doi:10.20944/preprints201810.0526.v1

nm. These are interpreted to be calcite and confirmed by XRD analysis (Figure 1C). Vaterite precipitates (Figure 1B) consist of spherical grains of 4-5 μm in diameter also accompanied by rhombohedral grains (4-5 μm), which are calcite according to the XRD scans (Figure 1C). Therefore, both ACC and vaterite precipitates are about 90% pure (from XRD analysis) with only minor amounts of calcite.

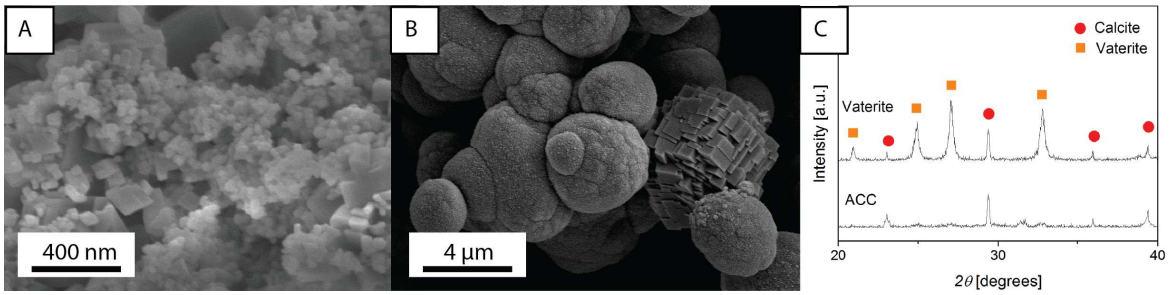


**Figure 1.** *SEM micrographs of synthesized calcium carbonate powders in the form of ACC phase (a) and Vaterite phase (b). XRD patterns (c) of lyophilized ACC and vaterite powders.*

*3.2. Phase transformation during setting and hardening*

The evolution of the cement compositions during the setting reaction has been followed by *in-situ* time-resolved XRD. Figure 2 includes the calculated molar fractions, $X_i$, of the three calcium carbonate polymorphs (ACC, vaterite and calcite) that coexist during the process for three different $CaCO_3$ cement compositions (1:1, 1:2 and 1:3 wt.% ACC:V) as well as for pure ACC (ACC:V 1:0) and pure vaterite (ACC:V 0:1) pastes as references. It shows visually how the two starting phases – ACC and vaterite – are dissolving while the third one – calcite – is growing at the expense of the other two.

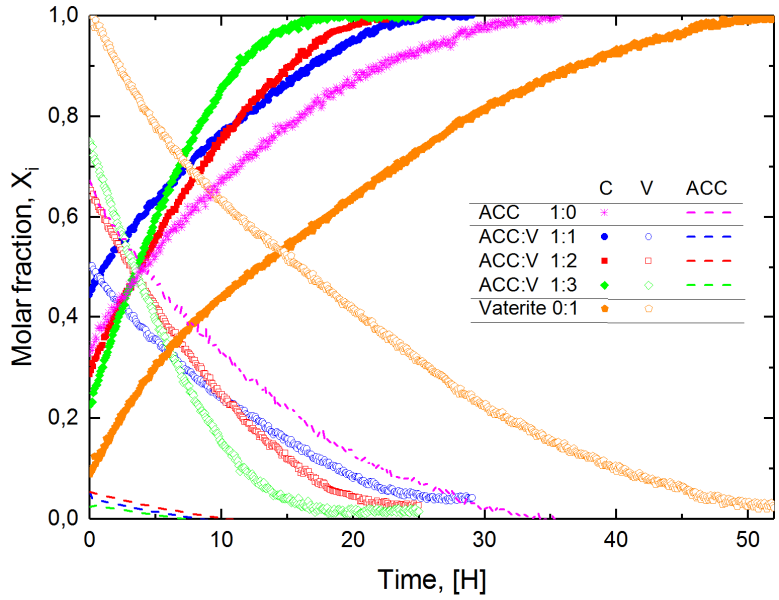


**Figure 2.** *Calcite, vaterite and ACC mole fractions, $X_i$, evolution with time for three different $CaCO_3$ cement compositions (1:1, 1:2 and 1:3 wt.% ACC:V). Pure ACC (1:0 wt.%) and vaterite (0:1 wt.%) pastes have been also included as references. Solid symbols represent calcite while empty symbols and dashed lines stand for vaterite and ACC, respectively.*

Preprints (www.preprints.org) | NOT PEER-REVIEWED | Posted: 23 October 2018 doi:10.20944/preprints201810.0526.v1

For the three cement compositions including ACC:V mixtures, the results show a clear trend: higher initial vaterite concentration leads to faster growth rates and shorter recrystallization process. However, pure vaterite (ACC:V 0:1 wt.%) shows the slowest transformation kinetics, probably due to its lower free-energy difference, $\Delta G$, (6.2 KJ/mol [29]) with respect to calcite in comparison with ACC (15.0 KJ/mol [14]). Hence, to rationalize this trend, the different phase transition kinetics must be considered and compared. Those can be described by the crystal growth rate, *r*, (also representing dissolution if it is negative) which is expressed as:

$$r = \pm K \cdot A \cdot e^{\frac{-E_a}{RT}} \cdot f(\Delta G) \quad (4)$$

where *K* is the growth rate constant (kg $s^{-1}$ $m^{-2}$), *A* is the reactive surface area of the growing phase, $E_a$ is the apparent activation energy of the overall reaction, *R* is the gas constant, *T* is the absolute temperature and $f(\Delta G)$ introduces the dependence of the overall growth rate on the supersaturation state of the system expressed as a function, *f*, of the Gibbs free-energy change for the growth reaction, $\Delta G$.

The $\Delta G$ function may have a variety of forms. However, since the overall reaction here presented is an elementary reaction, $f(\Delta G)$ can be derived from transition state theory (TST) [30,31] in the following way:

$$f(\Delta G) = \left(e^{\frac{\Delta G}{RT}} - 1\right)^n \approx \left(\frac{\Delta G}{RT}\right)^n \quad (5)$$

To identify the rate-determining step of ACC and vaterite transformation into calcite, the evolution of the mass, *m*, of each phase should be analysed and compared with the growth rate:

$$r = \frac{dm}{dt} = \pm K \cdot A \cdot \left(\frac{\Delta G}{RT}\right)^n \quad (6)$$

Assuming that the growth rate constant of the transformation, *K*, and the supersaturation, $\Omega = \Delta G/RT$, of the system does not change with time we can combine them into a single constant term, $\varphi = K\left(\frac{\Delta G}{RT}\right)^n$. Moreover, the mass of a particle, *m*, is proportional to the cube of its length, *L*, ($m \propto L^3$), whereas its area, *A*, is proportional to the square of its length, ($A \propto L^2$). Thus, the area is proportional to 2/3 of the mass: $A \propto m^{2/3}$. With those considerations, Eq. 6 results in:

$$\frac{dm}{dt} = \pm \varphi \cdot m^{2/3} \quad (7)$$

In this equation, the positive (resp. negative) sign is used to describe the time evolution of the calcite mass, $m_C$ (resp. the vaterite mass, $m_V$ ).

At this point, two antagonist hypotheses can be proposed to continue deriving Eq. 7. The former considers that calcite precipitation is limiting the transformation. Thus, considering the evolution of the mass of the newly formed calcite particles during the entire reaction length, Eq. 7 results in:

Preprints (www.preprints.org) | NOT PEER-REVIEWED | Posted: 23 October 2018 doi:10.20944/preprints201810.0526.v1

$$\int_{m_0}^{m} dm_C \cdot m_C^{2/3} = \int_0^t \varphi \cdot dt \tag{8}$$

$$3\left(m_C^{1/3} - {m_{C,0}}^{1/3}\right) = \varphi \cdot t \tag{9}$$

where $m_{c,0}$ is the initial calcite mass which is here equal to zero. Dividing Eq. 9 by $3{m_{C,0}}^{1/3}$, we get:

$$\frac{m_C}{m_{C,0}} = \frac{\varphi}{3\,{m_{C,0}}^{1/3}} \cdot t^3 = \left(\frac{t}{\tau}\right)^3 \tag{10}$$

where $\tau = 3{m_0}^{1/3}(RT/\Delta G)^n/K$. This suggests that the evolution of the mass of the growing calcite phase is proportional to the cube of time. Figure 3 shows this theoretical outcome along with the experimental evolution measured for the calcite phase from the different $CaCO_3$ cement samples (ACC:V wt.%) here studied. The results unequivocally show that calcite growth does not follow this hypothesis and therefore it is not the ruling-step of the transformation. This precipitation limited model agrees well with previous studies which report that the transformation of vaterite to calcite is dependent on the available surface area of calcite present. Even though similar power dependence with time was reported by *Ogino et al*. [8] and *Rodriguez-Blanco et al*. [11] for batch experiments, the transformation mechanism of $CaCO_3$ polymorphs within a cement paste is clearly different.

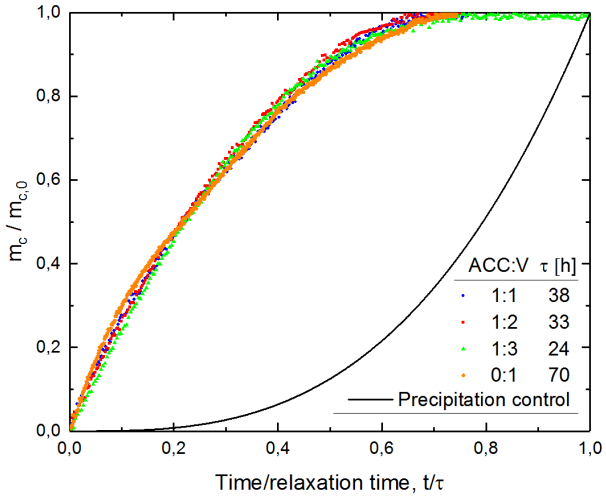


**Figure 3**. *Normalized calcite mass evolution with time for three different $CaCO_3$ cement compositions (1:1, 1:2 and 1:3 wt.% ACC:V) and pure vaterite paste (0:1 wt.% ACC:V). The solid line shows the outcome of the calcite precipitation model (Eq. 10).*

On the other hand, the opposite assumption considers that vaterite dissolution is the rate limiting step of the transformation. Under this assumption we may integrate Eq. 7 the same way as before and the evolution of the mass of the dissolving vaterite phase results to follow:

$$\frac{m_V}{m_{V,0}} = \left(1 - \frac{t}{\tau}\right)^3 \tag{11}$$

Preprints (www.preprints.org) | NOT PEER-REVIEWED | Posted: 23 October 2018 doi:10.20944/preprints201810.0526.v1

This theoretical interpretation is included on Figure 4A along with the experimental data measured for the vaterite phase from different cement pastes. The good agreement between the model and the data suggests that the transformation of vaterite to calcite within a cement paste system is limited by the dissolution of vaterite. There remains, however a small systematic deviation between the two.

We have established that vaterite dissolution is the rate limiting step. The composition of the liquid phase of the cement paste is therefore controlled by the solubility of calcite ($K_{sp,c} = 10^{-8.480}$ $M^2$) [29]. The Gibbs free energy difference between vaterite and calcite is $\Delta G' = RTln(K_{sp,v}/K_{sp,c})$, where $K_{sp,v} = 10^{-7.913}$ $M^2$ is the solubility product of vaterite.

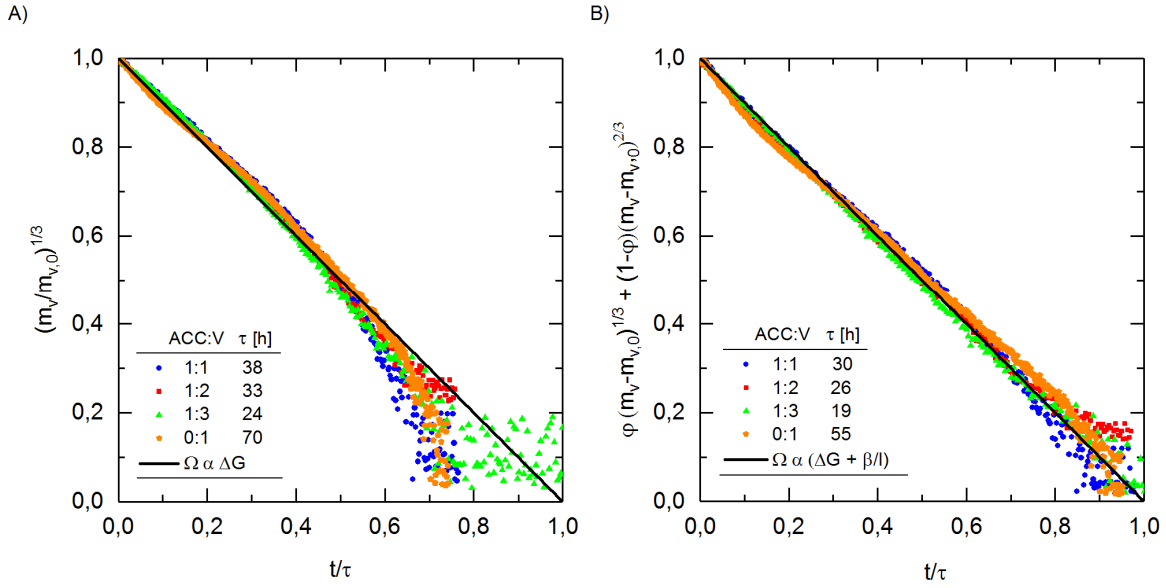


**Figure 4.** *Normalized vaterite mass evolution with time for three different $CaCO_3$ cement compositions (1:1, 1:2 and 1:3 wt.% ACC:V) and pure vaterite paste (0:1 wt.% ACC:V) considering: A) the supersaturation, Ω, proportional to the Gibbs free energy of the system ΔG, and B) the supersaturation, Ω, proportional to the Gibbs free energy of the system, ΔG, and the grain size, l, evolution. The solid line shows the outcome of the vaterite dissolution model under both situations [A) Eq.*11*, and B) Eq.*14*].*

The fit, however, still can be improved by considering the effect of the grain size change of both vaterite and calcite crystals during the transformation. The dissolution of vaterite particles reduces their size and changes the Laplace pressure of the particles in the paste. Consequently, the Gibbs energy difference, ΔG, between vaterite and calcite varies inversely proportional to the radius of the particles [32]:

$$\Delta G = \frac{2 \cdot \gamma \cdot \tilde{V}}{l} \tag{12}$$

where $\gamma$ is the surface tension of vaterite, $\tilde{V}$ is the total molar volume of vaterite and $l$ is the mean radius of the vaterite particles. Thus, with this extra particle size dependency, the evolution of the vaterite mass, $m_V$, includes an extra term within the growth rate equation:

$$\frac{dm_V}{dt} = -K\left(\frac{s^2 g N}{\rho}\right)^{1/3} \cdot m_V^{2/3} \cdot \left(\Omega + \left(\frac{gN}{s\rho}\right)^{1/3} \frac{2 \cdot \gamma \cdot \tilde{V}}{m_V^{1/3}}\right) \tag{13}$$

Preprints (www.preprints.org) | NOT PEER-REVIEWED | Posted: 23 October 2018 doi:10.20944/preprints201810.0526.v1

where N is the number of particles, $\rho$ the density of vaterite and $s$ and $g$ are geometrical factors ($s$=3 for a cube and 6 for a sphere and $g = 24$ for a cube and $g = 4\pi$ for a sphere).Thus, the evolution of the vaterite mass can be expressed as a simple function with the two constants $\alpha$ and $\beta$:

$$\frac{dm_V}{dt} = -\alpha \cdot m_V^{2/3} - \beta \cdot m_V{}^{1/3} \quad (14)$$

Figure 4B shows the best fit obtained for the vaterite dissolution model considering the contribution of the grain size change and its effect on the chemical potential. Including this contribution within the model yields to lowered time constant values, $\tau$, being $\tau_{ACC:V\ 1:1}$ = 30 h, $\tau_{ACC:V\ 1:2}$ = 26 h, $\tau_{ACC:V\ 1:3}$ = 19 h and $\tau_{ACC:V\ 0:1}$ = 55 h.

Previous phase transformation studies in well stirred liquid solutions agreed to claim that the major driving force behind rapid ACC and moderate vaterite dissolution is the growth of more stable polymorphic forms [8,33]. Moreover, their transformation mechanisms are dissimilar when they are in solutions: while vaterite conversion takes place through its dissolution and subsequent recrystallization into the most stable calcite phase [34], the transformation of ACC into crystalline phases occur via direct (solid phase conversion) and indirect (dissolution & precipitation) transformation pathways simultaneously [15]. We have pointed out a clear difference between transformation in solution and in a cement paste, but it is outside the scope of this study to propose a new, detailed transformation mechanism within a cement paste. It is clear however that the time constant $\tau \propto \frac{1}{K\Omega}\left(\frac{m_{V,0}}{N}\right)^{1/3}$ changes for the different compositions of the initial cement mixture. The initial mean particle size, $r \propto (m_0/N)^{1/3}$, should be independent of the initial mixture ratio. The supersaturation, $\Omega$, is affected by the solubility of ACC that is higher than that of vaterite. Therefore the dissolution of vaterite will be stopped or slowed down locally where in contact with ACC. We will not attempt to model this because it is a complex function of cement structure, diffusion and will evolve with the amount of ACC left. We do note, however that the time constant should become larger as ACC content is increased, in line with the measured time constants for the intermediate concentrations 1:1, 1:2 and 1:3. What remains to be explained is why vaterite transformation is much faster when there is ACC present than when there is no ACC. We can only propose that this may be due to some catalytic effect of an intermediate $CaCO_3$ phase present when there is ACC in the mixture and that this increases the rate constant K.

*3.3. Viscoelasticity of $CaCO_3$ pastes*

Figure 5 includes the time evolution of the storage modulus, *G'*, over 10 hours for three different $CaCO_3$ cement pastes. For each composition, we collect on Figure 7 the two most dissimilar evolutions that have been measured to show the maximum deviation rather than error bars. The storage modulus, *G'*, is typically one order of magnitude larger than the loss modulus, *G''*, revealing the elastic-like behavior of the pastes (not shown). One can observe that the initial rigidity of the pastes is different depending on the composition and increases with the Vaterite/ACC ratio. The reason might be attributed to the larger dimension of vaterite particles in comparison with ACC particles (one order of magnitude; Figure 1).

Preprints (www.preprints.org) | NOT PEER-REVIEWED | Posted: 23 October 2018 doi:10.20944/preprints201810.0526.v1

This kind of dependence has been reported previously not only for cement pastes but for several systems [35,36].

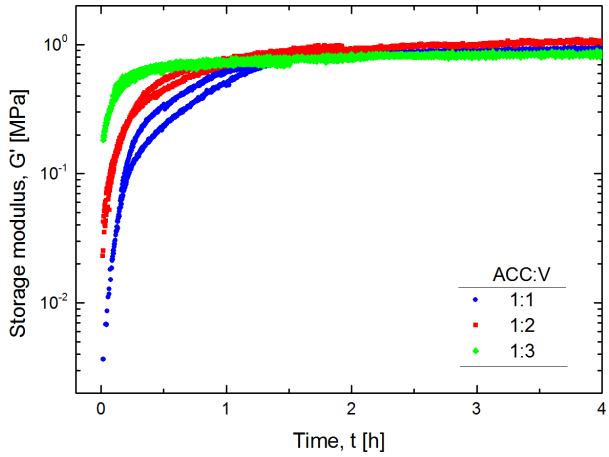


**Figure 5.** *Evolution of storage modulus, G', with time of three different $CaCO_3$ cement compositions (1:1, 1:2 and 1:3 wt.% ACC:V) measured from aging experiments (constant frequency, f=10 Hz, and deformation, $\gamma$=0.003%).*

For all studied pastes, the storage modulus, *G'*, increases progressively with time until it reaches a value of ~ 0.7 MPa independently of the composition. It is remarkable that even though all the original solid material in the paste is dissolved the storage modulus never decreases. This trend suggests that the main changes of the structural built-up mechanism occur within the early stages of maturation, i.e., just after mixing the ACC and vaterite with water, whereas a secondary mechanism continues developing the microstructure within the following hours. Further insights from the data included on Figure 5 can be extracted by normalizing the storage modulus:

$$G'_N = \frac{G'(t_f) - G'(t)}{G'(t_f) - G'(t_0)} \quad (15)$$

Figure 6 shows the evolution with time of the normalized storage modulus, $G'_N$, for the three different $CaCO_3$ cement pastes examined. One observes two distinctive periods of building up strength; first a fast (steep slope) then a slow (small slope). These are characterized by their relaxation times, $\tau'_i$, which basically stand for the time required for the storage modulus to reduce to 1/e of its original value. Thus, they can be determined by fitting the specific ranges into the following equation:

$$\ln G'_N = -t/\tau'_i \quad (16)$$

where *t* represents the time. For the initial short-range step, the calculated characteristic reaction times, $\tau'_1$, are 2.30 h, 1.60 h and 0.88 h, whereas for the secondary long-range step, $\tau'_2$, the values are 12 ± 2 h, 12 ± 2 h and 10 ± 2 h for ACC:V 1:1, 1:2 and 1:3 compositions, respectively.

Preprints (www.preprints.org) | NOT PEER-REVIEWED | Posted: 23 October 2018 doi:10.20944/preprints201810.0526.v1

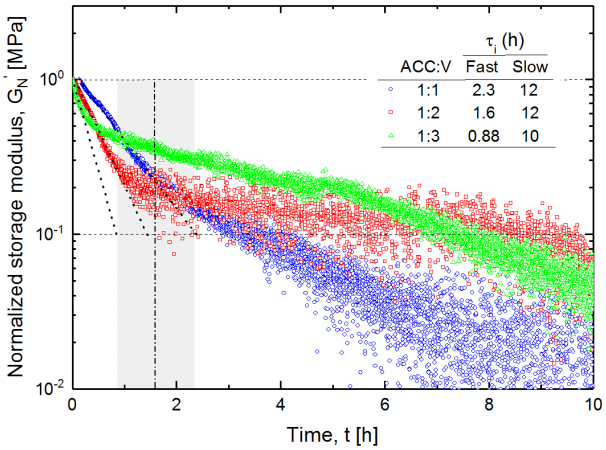


**Figure 6.** *Evolution of the normalized storage modulus, $G_N$', with time for three different $CaCO_3$ cement compositions (1:1, 1:2 and 1:3 wt.% ACC:V) measured from aging experiments. The average characteristic reaction times, $\tau_i$', extracted from Eq.*16 *for each step are also included.*

The rheology of fresh cement pastes is a complex field and involves a full range of forces and transformations at the microstructural level, which in some way determine the evolution of the measured parameters [37]. For cementitious suspensions having a polydisperse distribution of particles, three types of inter-particle forces may exist including: i) hydrodynamic; ii) Brownian; and iii) colloidal forces [38]. The former - hydrodynamic (or viscous) forces - exist in all suspensions since they arise from the relative motion of particles with respect to the surrounding fluid. Brownian force is always present and represents a thermal randomizing force; and colloidal forces are potential forces with elastic and electrostatic nature [39]. The relative magnitude among these forces depends on the particle size of the suspension although for cementitious pastes the rheological behavior is mainly dominated by the inter-particle colloidal forces [40].

In order to support a finite amount of stress without flow, $CaCO_3$ cement pastes must possess an internal network of particles with attractive interactions either via direct contacts or via colloidal forces (van der Waals) [40]. Several mechanisms have been reported for OPC pastes to rationalize how a flocculated network starts to develop its structural integrity [41,42]. Among those, some of them seem to be compatible with the captured evolutions for $CaCO_3$ cements. For example, the raise of the rigidity of the pastes within the initial short-range step can be interpreted as the geometrical redistribution of both ACC and vaterite particles within the paste until they get in contact. This process takes place here on the order of the hour (from 0.9 and 2.3h), suggesting the existence of an electrostatic barrier between colloidal particles. Indeed for colloids interacting solely through Van der Waals, we can expect a diffusive time over their size (R~µm) of typically 1 s smaller than the measured characteristic times. The diverse particle size distribution (PSD) of each cement composition may also explain the differences within them [40]. Simultaneously, the (re)crystallization of both phases is also taking place since the powders are mixed with water, as it has been shown on the previous section, but probably their contribution is not large enough to induce such remarkable climbs on the paste rigidity. Indeed, this (re)crystallization process seems to be the responsible mechanism for the strengthening advance during

Preprints (www.preprints.org) | NOT PEER-REVIEWED | Posted: 23 October 2018 doi:10.20944/preprints201810.0526.v1

the secondary long-term structural development. Once the solid phases (former ACC and vaterite particles plus the newly formed calcite crystals) are in contact the (re)crystallization continues inducing growth of former calcite crystals rather than nucleating new ones, as described by the Ostwald ripening or competitive growth phenomena [43,44]. Thus, the structural built up of $CaCO_3$ pastes during this phase is probably due to the development of crystals joints, also known as "bridging effect" or "crystal entanglement" [45]. How this process evolves with time not only depends on the particular (re)crystallization kinetics and energetics of both ACC and vaterite phases into calcite but on their relative amount within the pastes since, as shown on the previous section, this parameter determines the driving force of the transformation.

Figure 7 presents the evolution of the storage modulus, *G'*, as function of the strain, γ, for the three ACC:V analyzed compositions, after 5 hours of reaction. The extracted linear storage modulus, $G'_{lin}$, are 1.05 MPa, 1.31 MPa and 0.73 MPa for the 1:1, 1:2 and 1:3 wt.% ACC:V compositions, respectively. These values, which are not statistically different, are not far away from the maximum values acquired after 1 hour of aging. Hence, this supports the fact that the main rearrangements of the different $CaCO_3$ particles to establish an entangled network takes place within the early stages of maturation, whereas this process continues via crystal bridging on a slower manner within the following hours. In addition, those values also show that the setting and hardening dynamics are progressing without been disturbed by the oscillatory deformation, as expected.

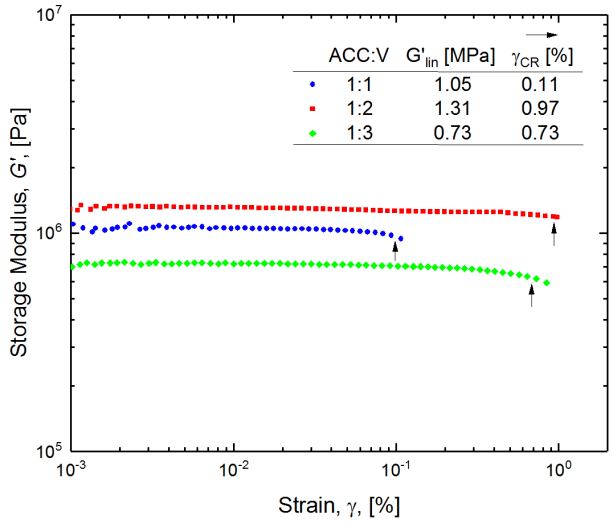


**Figure 7.** *Linear storage modulus, $G'_{lin}$, versus deformation, γ, of three different $CaCO_3$ cement compositions (1:1, 1:2 and 1:3 wt.% ACC:V) measured from amplitude sweep experiments (constant frequency, f=10 Hz, increasing stress, 0-$10^4$ Pa). The extracted linear storage modulus, $G'_{lin}$, and the critical strain, $\gamma_{cr}$, are also included within the legend. The arrows indicate the position of the critical strain, $\gamma_{cr}$, for each composition.*

The results also show that the critical strain, $\gamma_{cr}$, required to bring the ACC:V 1:1 paste into the plastic regime is considerably lower (~0.1%) than that for the other two compositions (~1%). This fact might be interpreted as a signal of lower rigidity development, i.e, a less efficient (or slower) bridging effect. Indeed, this result is consistent with the characteristic reaction times, $\tau_i$, calculated from the XRD

Preprints (www.preprints.org) | NOT PEER-REVIEWED | Posted: 23 October 2018 doi:10.20944/preprints201810.0526.v1

analysis. The ACC:V 1:1 paste shows the largest characteristic reaction time ($\tau_{1.1}$ = 30 h) among the ACC:V tested compositions, resulting therefore on a slower bridging development. Thus, these results underscore again the importance of the relative amount of ACC, vaterite and calcite particles that coexist along the setting reaction, since it determines or regulates how the joints between them can be formed and will determine the final mechanical properties of the set samples.

A comparison between the characteristic (re)crystallization time, $\tau_i$, measured from XRD analysis and the characteristic build up times, $\tau_i'$, measured from rheological experiments is included on Figure 8. As can be observed, both characteristic build-up times, $\tau_i'$, follow a linear relationship with the characteristic (re)crystallization time, $\tau$. Thus, these results indicates that the increase on the (re)crystallization extent is directly correlated with the progression of the structural development of the paste. The initial short-range characteristic time yields $\tau_1' = 0.13 \cdot \tau - 1.65$, whereas the long-range characteristic time holds $\tau_2' = 0.19 \cdot \tau + 6.49$. Therefore, these results shows that the (re)crystallization contributes to the structural development of the paste into a solid during the entire setting reaction but with a more evident contribution during the secondary long-range step.

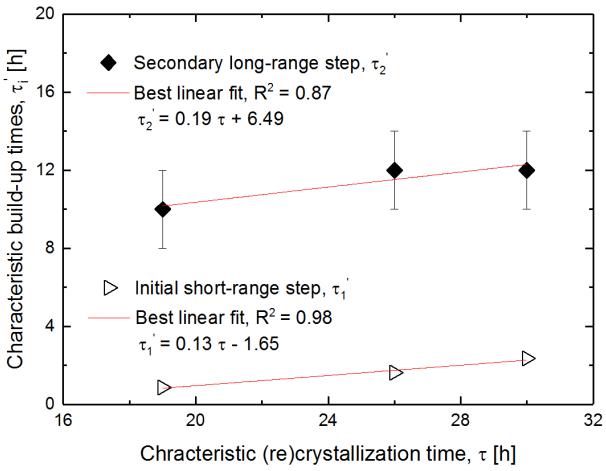


**Figure 8.** *Correlation between the characteristic (re)crystallization time, τ, and the characteristic build-up times, $\tau_i'$ measured from XRD and rheological experiments, respectively, for three different $CaCO_3$ cement compositions (1:1, 1:2 and 1:3 wt.% ACC:V).*

## 4. Conclusions

The transformation kinetics of all $CaCO_3$ polymorphs that coexist during the cement setting reaction has been studied in pure pastes (ACC:V 0:1 and 1:0) and within cement mixtures (ACC:V 1:1, 1:2 and 1:3). Although amorphous calcium carbonate and vaterite pastes show the slowest (re)crystallization kinetics ($\tau_{ACC:V\ 0:1}$ = 55 h), their combination to synthesize cements results in faster transformations dominated by the initial amount of vaterite ($\tau_{ACC:V\ 1:1}$ = 30 h, $\tau_{ACC:V\ 1:2}$ = 26 h and $\tau_{ACC:V\ 1:3}$ = 19 h). The progress of the transformation within a cement paste system is controlled by the dissolution of vaterite, and the supersaturation, Ω, depends not only on the free energy difference of the system, ΔG, but on the grain size evolution.

The main mechanism for building structural strength of calcium carbonate cement occurs within the early stages of maturation (average $\tau_1' = 1.6 \pm 0.7$ h) and deals with the geometric reorganization of $CaCO_3$ particles within the paste until they get in contact. A secondary mechanism is based on the development of joints within the nucleated calcite crystals in order to form an interconnected network. It acts during the whole length of the setting reaction (average $\tau_2' = 11 \pm 3$ h) but more strongly once the previous step is over. A direct comparison between the characteristic (re)crystallization time, $\tau_i$, and the characteristic strengthening times, $\tau_i'$, indicates that the increase on the (re)crystallization extent is directly correlated with the progression of the structural development of strength in the paste.

By the end of the setting reaction, cements of all initial compositions are entirely made of entangled calcite crystals, with varying extent of crystal bridging. Thus, dissimilar mechanical performance is expected for these cements.

**Acknowledgments**

This project has received funding from the European Union Horizon 2020 research and innovation program under the Marie Skłodowska-Curie grant agreement no. 642976-NanoHeal Project. The results of this paper reflect only the author's view and the Commission is not responsible for any use that may be made of the information it contains. The authors would like to express gratitude to the late Ellis Gartner who suggested the preparation protocol studied here and that contributed through many discussions. J.R.-S. would like to express his thanks to Lab engineer David Wragg (University of Oslo) for his assistance analyzing XRD data and to Professors Jean Colombani and Marie Le Merrer (University of Lyon) for their fruitful discussions.

**References**

[1] E.M. Gartner, D.E. Macphee, A physico-chemical basis for novel cementitious binders, Cem. Concr. Res. 41 (2011) 736–749. doi:10.1016/j.cemconres.2011.03.006.
[2] J.L. Provis, J.S.J. van Deventer, Alkali Activated Materials, Springer, 2014.
[3] T. Zhang, C.R. Cheeseman, L.J. Vandeperre, Development of low pH cement systems forming magnesium silicate hydrate (M-S-H), Cem. Concr. Res. 41 (2011) 439–442. doi:10.1016/j.cemconres.2011.01.016.
[4] H. Justnes, Alternative Low-CO2 "Green" Clinkering Processes, Rev. Mineral. Geochemistry. 74 (2012) 83–99. doi:10.2138/rmg.2012.74.2.
[5] M.-L. Fontaine, C. Combes, T. Sillam, G. Dechambre, C. Rey, New Calcium Carbonate-Based Cements for Bone Reconstruction, Key Eng. Mater. 284–286 (2005) 105–108. doi:10.4028/www.scientific.net/KEM.284-286.105.
[6] C. Combes, B. Miao, R. Bareille, C. Rey, Preparation, physical-chemical characterisation and cytocompatibility of calcium carbonate cements, Biomaterials. 27 (2006) 1945–1954. doi:10.1016/j.biomaterials.2005.09.026.
[7] D. Zaelke, O. Young, S.O. Andersen, Scientific synthesis of Calera carbon sequestration and carbonaceous by-product applications. Consensus findings of the scientific synthesis team, (2011).
[8] T. Ogino, T. Suzuki, K. Sawada, The formation and transformation mechanism of calcium carbonate in water, Geochim. Cosmochim. Acta. 51 (1987) 2757–2767. doi:10.1016/0016-7037(87)90155-4.
[9] J. Wang, U. Becker, Energetics and kinetics of carbonate orientational ordering in vaterite calcium carbonate, Am. Mineral. 97 (2012) 1427–1436. doi:10.2138/am.2012.3990.
[10] J.P. Andreassen, Formation mechanism and morphology in precipitation of vaterite - Nano-

aggregation or crystal growth?, J. Cryst. Growth. 274 (2005) 256–264. doi:10.1016/j.jcrysgro.2004.09.090.
[11] J.D. Rodriguez-Blanco, S. Shaw, L.G. Benning, The kinetics and mechanisms of amorphous calcium carbonate (ACC) crystallization to calcite, via vaterite, Nanoscale. 3 (2011) 265–271. doi:10.1039/c0nr00589d.
[12] P. Bots, L.G. Benning, J.-D. Rodriguez-Blanco, T. Roncal-Herrero, S. Shaw, Mechanistic insights into the crystallization of amorphous calcium carbonate (ACC), Cryst. Growth Des. 12 (2012) 3806–3814. doi:10.1021/cg300676b.
[13] F. Konrad, F. Gallien, D.E. Gerard, M. Dietzel, Transformation of Amorphous Calcium Carbonate in Air, Cryst. Growth Des. 16 (2016) 6310–6317. doi:10.1021/acs.cgd.6b00906.
[14] G. Wolf, C. Günther, Thermophysical investigations of the polymorphous phases of calcium carbonate, J. Therm. Anal. Calorim. 65 (2001) 687–698. doi:10.1023/A:1011991124181.
[15] M.H. Nielsen, S. Aloni, J.J. De Yoreo, In situ TEM imaging of CaCO3 nucleation reveals coexistence of direct and indirect pathways, Science (80-. ). 345 (2014) 1158–1162. doi:10.1126/science.1254051.
[16] B.B. Schroeder, D.D. Harris, S.T. Smith, D.O. Lignell, Theoretical framework for multiple-polymorph particle precipitation in highly supersaturated systems, Cryst. Growth Des. 14 (2014) 1756–1770. doi:10.1021/cg401892b.
[17] F.P. Carr, D.K. Frederick, Calcium carbonate, in: Kirk-Othmer (Ed.), Kirk-Othmer Encycl. Chem. Technol. Vol. 1 - 26, 5th Ed., John Wiley & Sons, Inc, 1967: pp. 551–556.
[18] J.L. Banner, Application of the trace element and isotope geochemistry of strontium to studies of carbonate diagenesis, Int. Assoc. Sedimentol. 42 (1995) 805–824.
[19] H. Colfen, Precipitation of carbonates: recent progress in controlled production of complex shapes, Curr. Opin. Colloid Interface Sci. 8 (2003) 23–31. doi:10.1016/S1359-0294.
[20] P.O. Roehl, P.W. Choquette, Carbonate Petroleum Reservoirs, 1985. doi:10.1007/978-1-4612-5040-1.
[21] A. V. Radha, T.Z. Forbes, C.E. Killian, P.U.P.A. Gilbert, A. Navrotsky, Transformation and crystallization energetics of synthetic and biogenic amorphous calcium carbonate, Proc. Natl. Acad. Sci. 107 (2010) 16438–16443. doi:10.1073/pnas.1009959107.
[22] S.E. Wolf, C.F. Bohm, J. Harris, B. Demmert, D.E. Jacob, M. Mondeshki, E. Ruiz-Agudo, C. Rodriguez-Navarro, Nonclassical crystallization in vivo et in vitro (I): Process-structure-property relationships of nanogranular biominerals, J. Struct. Biol. 196 (2016). doi:10.1016/j.jsb.2016.07.016.
[23] J.Y. Gal, J.C. Bollinger, H. Tolosa, N. Gache, Calcium carbonate solubility: A reappraisal of scale formation and inhibition, Talanta. 43 (1996) 1497–1509. doi:10.1016/0039-9140(96)01925-X.
[24] R.J. Flatt, N.S. Martys, L. Bergström, The Rheology of Cementitious Materials, 29 (2004) 314–318.
[25] K. Yamada, S. Ogawa, S. Hanehara, Controlling of the adsorption and dispersing force of polycarboxylate-type superplasticizer by sulfate ion concentration in aqueous phase, Cem. Concr. Res. 31 (2001) 375–383. doi:10.1016/S0008-8846(00)00503-2.
[26] T. Liberto, M. Le Merrer, C. Barentin, M. Bellotto, J. Colombani, Elasticity and yielding of a calcite paste: scaling laws in a dense colloidal suspension, Soft Matter. 13 (2017) 2014–2023. doi:10.1039/C6SM02607A.
[27] Weitz, D. A., Diffusing Wave Spectroscopy, Dyn. Light Scatt. Method Some Appl. (1993) 652–720.
[28] R.G. Larson, The Structure and Rheology of Complex Fluids, Oxford Univ. Press, Oxford and New York, 1999. http://ci.nii.ac.jp/naid/110002077498/en/.
[29] L.N. Plummer, E. Busenberg, The solubilities of calcite, aragonite and vaterite in CO-H2O solutions between 0 and 9OC, and an evaluation of the aqueous model for the system CaC03-CO2-H20, Gcochlmica Cosmochim. Acta. 46 (1982) 1011–1040.
[30] A.C. Lasaga, Volume 8: Kinetics of Geochemical Processes, in: A.C. Lasaga, R.J. Kirkpatrick (Eds.), Kinet. Geochemical Process., Mineralogical Society of America, Urbana, Illinois, USA, 1981: p. 81.
[31] P. Aagaard, H.C. Helgeson, Thermodynamic and kinetic constraints on reaction rates among minerals and aqueous solutions. I. Theoretical considerations., Am. J. Sci. 282 (1982) 237–285.

doi:10.2475/ajs.282.3.237.
[32] K. Graf, M. Kappl, Physics and chemistry of interfaces, John Wiley & Sons, Ltd, Berlin, 2006.
[33] B.B. Schroeder, D.D. Harris, S.T. Smith, D.O. Lignell, Theoretical framework for multiple-polymorph particle precipitation in highly supersaturated systems, Cryst. Growth Des. 14 (2014) 1756–1770. doi:10.1021/cg401892b.
[34] D. Kralj, L. Brecević, A.E. Nielsen, Vaterite growth and dissolution in aqueous solution II. Kinetics of dissolution, J. Cryst. Growth. 143 (1994) 269–276. doi:10.1016/0022-0248(94)90067-1.
[35] L. Hernández, M. Gurruchaga, I. Goñi, Influence of powder particle size distribution on complex viscosity and other properties of acrylic bone cement for vertebroplasty and kyphoplasty, J. Biomed. Mater. Res. - Part B Appl. Biomater. 77 (2006) 98–103. doi:10.1002/jbm.b.30409.
[36] B.E. Larsen, J. Bjørnstad, E.O. Pettersen, H.H. Tønnesen, J.E. Melvik, Rheological characterization of an injectable alginate gel system, BMC Biotechnol. 15 (2015) 1–12. doi:10.1186/s12896-015-0147-7.
[37] D. Jiao, C. Shi, Q. Yuan, X. An, Y. Liu, H. Li, Effect of constituents on rheological properties of fresh concrete-A review, Cem. Concr. Compos. 83 (2017) 146–159. doi:10.1016/j.cemconcomp.2017.07.016.
[38] J.M. Brader, Nonlinear rheology of colloidal dispersions, J. Phys. Condens. Matter. 22 (2010) 363101–363137. doi:10.1088/0953-8984/22/36/363101.
[39] S.B. Johnson, G. V Franks, P.J. Scales, D. V Boger, T.W. Healy, Surface chemistry – rheology relationships in concentrated mineral suspensions, Int. J. Miner. Process. 58 (2000) 267–304.
[40] N. Roussel, A. Lemaître, R.J. Flatt, P. Coussot, Cement and Concrete Research Steady state fl ow of cement suspensions : A micromechanical state of the art, Cem. Concr. Res. 40 (2010) 77–84. doi:10.1016/j.cemconres.2009.08.026.
[41] M.A. Schultz, L.J. Struble, Use of oscillatory shear to study flow behavior of fresh cement paste, Cem. Concr. Res. 23 (1993) 273–282. doi:10.1016/0008-8846(93)90092-N.
[42] Y. Zhang, X. Kong, L. Gao, Z. Lu, S. Zhou, B. Dong, F. Xing, In-situ measurement of viscoelastic properties of fresh cement paste by a microrheology analyzer, Cem. Concr. Res. 79 (2016) 291–300. doi:10.1016/j.cemconres.2015.09.020.
[43] W. Ostwald, “Studien über die Bildung und Umwandlung fester Körper” [Studies on the formation and transformation of solid bodies], Zeitschrift Für Phys. Chemie. 22 (1897) 289–330.
[44] P.W. Voorhees, The theory of Ostwald Ripening, J. Stat. Phys. 38 (1985) 231–252. doi:10.1007/BF01017860.
[45] C. Combes, S. Tadier, H. Galliard, S. Girod-Fullana, C. Charvillat, C. Rey, R. Auzely-Velty, N. El Kissi, Rheological properties of calcium carbonate self-setting injectable paste, Acta Biomater. 6 (2010) 920–927. doi:10.1016/j.actbio.2009.08.032.